ARCHIVIO ISTITUZIONALE
DELLA RICERCA

Alma Mater Studiorum Università di Bologna
Archivio istituzionale della ricerca

Efficient Bulk-Heterojunction Solar Cells Based on Symmetrically Disubstituted Polyalkyloxythiophenes at Low Synthetic Complexity

This is the final peer-reviewed author's accepted manuscript (postprint) of the following publication:

Published Version:
Lanzi, M., Pierini, F., Medri, R., Salatelli, E., Marinelli, M. (2025). Efficient Bulk-Heterojunction Solar Cells Based on Symmetrically Disubstituted Polyalkyloxythiophenes at Low Synthetic Complexity. MACROMOLECULAR CHEMISTRY AND PHYSICS, 226(17), 1-12 [10.1002/macp.202500184].

Availability:
This version is available at: https://hdl.handle.net/11585/1018506 since: 2025-06-27

Published:
DOI: http://doi.org/10.1002/macp.202500184

Terms of use:

Some rights reserved. The terms and conditions for the reuse of this version of the manuscript are specified in the publishing policy. For all terms of use and more information see the publisher's website.

This item was downloaded from IRIS Università di Bologna (https://cris.unibo.it/).
When citing, please refer to the published version.

(Article begins on next page)

06 November 2026

Efficient Bulk-Heterojunction Solar Cells Based on Symmetrically Disubstituted Polyalkyloxythiophenes at Low Synthetic Complexity

Massimiliano Lanzi[a,*], Filippo Pierini[b], Riccardo Medri[a], Elisabetta Salatelli[a], Martina Marinelli[a]

[a] *Dpt. of Industrial Chemistry "Toso Montanari", University of Bologna, Via Gobetti 85, 40129 Bologna, Italy.*

[b] *Dpt. of Biosystem and Soft Matter, Institute of Fundamental Technological Research, IPPT-PAN, Polish Academy of Science, ul. Pawińskiego 5B, 02-106 Warsaw, Poland.*

*Corresponding author: massimiliano.lanzi@unibo.it (M. Lanzi)

Keywords: polymeric solar cells, thiophene-based electron donors, alkyl side chain modification, figure of merit

ABSTRACT

The aim of this study is to present a challenging insight into the molecular design and architecture optimization of two cost-effective conjugated polymers and their adoptions in bulk heterojunction fullerene-based solar cells. The new polymers, with repeating units based on symmetrically disubstituted polyalkyloxythiophenes have been prepared with simple procedures and have been employed as electron-donor materials for polymer solar cells. A comparative study with a monosubstituted polyalkyloxythiophene has evidenced a more favorable active morphology, improved charge mobility and higher power conversion efficiency for the newly prepared disubstituted polymers. Photoconversion ability further increases when a thin layer of a cationic polyelectrolyte was coated on the surface of the photoactive blend, thus facilitating the electron transport. Finally, the prepared polymers were evaluated according to a figure of merit based on their synthetic complexity and conversion efficiency, resulting particularly suitable for large scale production.

1. Introduction

π-Conjugated polymers (CPs) show intriguing physical and chemical properties deriving from the alternating single and double C-C bonds in their macromolecular backbone. Electron delocalization along the polymer chain allows charge transport, making CPs valuable materials for several applications such as light-emitting diodes (LEDs), thin-film transistors (TFTs) and organic photovoltaic solar cells (OPVs) [1]. The selection of the right monomer for the final CP is of utmost importance since repeating units, directly deriving from the monomer structure, can effectively modify the chemical, electronic, and optical properties of the synthesized material. The photovoltaic process is composed of many subsequent steps: photon absorption, exciton creation, charge separation and transport to the electrode. Bulk heterojunction (BHJ) OPV cells are the most studied devices due to their simple and efficient architecture which allows good photoconversion efficiency and easy

assembling. In this structure, the photoactive layer is composed of a blend of an electron-donor (ED) polymer and an electron-acceptor (EA) molecule, properly chosen to assure a high interfacial area and an extended bicontinuity. The first studies regarding BHJs were focused on the use of a regioregular poly(3-alkylthiophene) (P3HT) as ED semiconducting material, owing to its extended π-delocalization, high thermal and environmental stability and synthetic easiness, blended with a fullerene derivative like [6,6]-phenyl-C_{61}butyric acid methyl ester ($PC_{61}BM$) [2]. However, despite P3HT affordability, it lacks absorption in the near-infrared and infrared regions of solar spectrum, since its absorption is limited to the visible region (350-550 nm) giving an evident loss of solar energy. On the other hand, polyalkylthiophenes can be easily functionalized with other chemical functional groups, adding the intrinsic properties of the substituent to those typical of the polyconjugated backbone. For example, oligomethylenic side chains bearing a methoxy group at the end of the alkylic chains gave excellent polymer solubility in common organic solvents and appreciable self-assembling capabilities when in the solid (film) state [3-4]. Moreover, if compared to the alkylic substituents, alkyloxy side chains directly linked to the 3-position of the thiophenic units can effectively increase the electron-injection to the backbone, thus lowering the bandgap of the ED polymer and enhancing the charge-transfer to the electron-acceptor (EA) counterpart in OPV solar cells [5-6]. Nevertheless, incorporation of alkyloxy groups consequently improves the exploitation of sunlight by increasing the absorption in the longer wavelength region [7].

In this work, two thiophenic monomers 3,4-disubstituted with alkyloxy side chains ended by methoxy groups were synthesized and polymerized through oxidative polymerization with iron trichloride. Due to the symmetry of the monomers, the prepared polymers were completely regioregular and were obtained with good molar mass, high yield, low polydispersity and, above all, by means of a straightforward and easy polymerization procedure, able to reduce the synthetic complexity of the final material. The two polymers, poly[3,4-bis(6-methoxyhexyl-1-oxy)thiophene] (**P1**) and poly[3,4-bis(10-methoxydecyl-1-oxy)thiophene] (**P2**), reported in Figure 1, have been employed as ED active layers in OPV solar cells, in combination with $PC_{61}BM$ as EA material. Their photovoltaic parameters have been compared with those of a reference polymer, i.e. the monosubstituted poly[3-(6-methoxyhexyl-1-oxy)thiophene] (**PR**), properly prepared to investigate the effects of the degree of substitution on the polymer final properties.

Moreover, some authors recently reported that singly-methylated imidazolium-functionalized polythiophenes have been applied as electrode interlayers in conventional and inverted organic solar cells, improving their performance.[8-9] In view of this, the cells photoconversion efficiency has also been evaluated in presence of a thin layer of the cationic polyelectrolyte poly{3-[6-(1-methylimidazolium-3-yl)hexyl]thiophene bromide} (**P3**, Figure 1), properly synthesized and inserted between the photoactive layer and the Al cathode. Finally, the Synthetic Complexity (SC) index has been calculated for all the polymers, to verify if the proposed syntheses could be scalable to produce OPV modules on an industrial scale, according to the method proposed by R. Po et al. for organic solar cells [10].

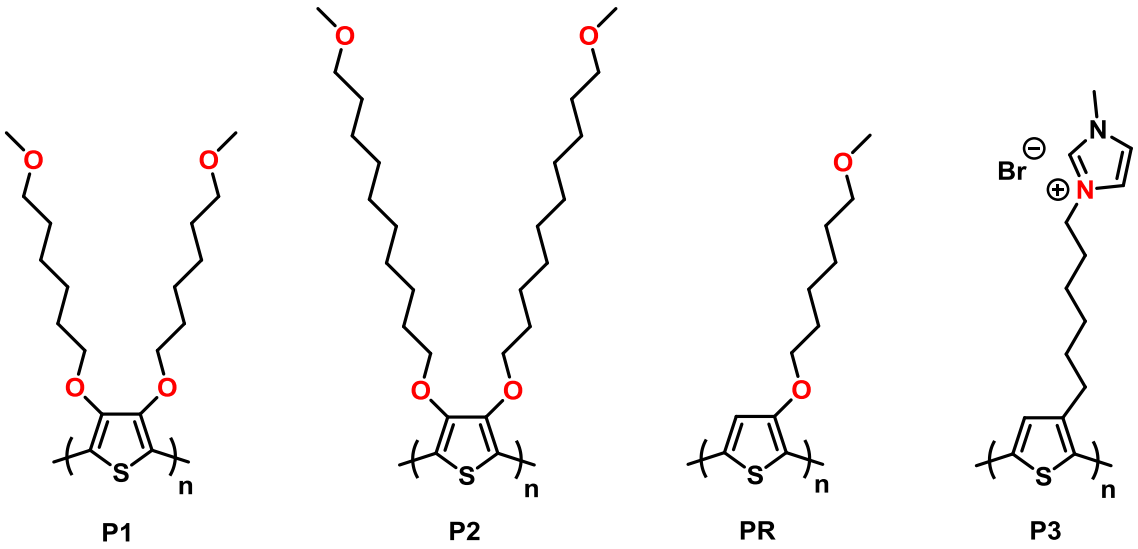

Figure 1. Overview of the synthesized polymers: electron-donor (ED) materials (**P1**, **P2** and the reference **PR**) and polyelectrolyte (**P3**).

2. Results and Discussion

2.1 Synthesis and Physical Characterization

Disubstituted alkyloxy-thiophene precursors **1a** and **2a** (Scheme 1) were obtained by transetherification reaction between 3,4-dimethoxythiophene and the corresponding synthetized alkylic chain (6-bromo-1-hexanol or 10-bromo-1-decanol, respectively) [11]. Due to the presence of the bromine group at the end of side chain, precursors could be easily functionalized by SN_2 reaction with a sodium methoxide solution (NaOMe 30% in MeOH), providing the desired monomers 3,4-bis(6-dimethoxyhexyl-1-oxy)thiophene (**1b**) and 3,4-bis(10-dimethoxydecyl-1-oxy)thiophene (**2b**). Monomers were subsequently polymerized with $FeCl_3$ in dry chloroform, to obtain the corresponding polymers poly[3,4-bis(6-methoxyhexyl-1-oxy)thiophene] (**P1**) and poly[3,4-bis(10-methoxydecyl-1-oxy)thiophene] (**P2**) (Scheme 1). The reference monosubstituted polymer **PR** was prepared starting from 3-methoxythiophene and 6-bromo-1-hexanol, then the obtained monomer TO6Br was dibrominated in the 2,5-positions of the aromatic ring, giving the intermediate BTO6Br, which was polymerized using the Grignard Metathesis Polymerization (GRIM) described by R. D. McCullough et al. [12]. The regioregular polymer PTO6Br (98% HT dyads) was then subjected to a post-polymerization functionalization (PPF) procedure. Basically, the bromide atom at the end of the side chain has been subjected to a nucleophilic substitution with methoxy group, leading to the polymer **PR** (Scheme 1). All synthetic details are given in Supporting Information.

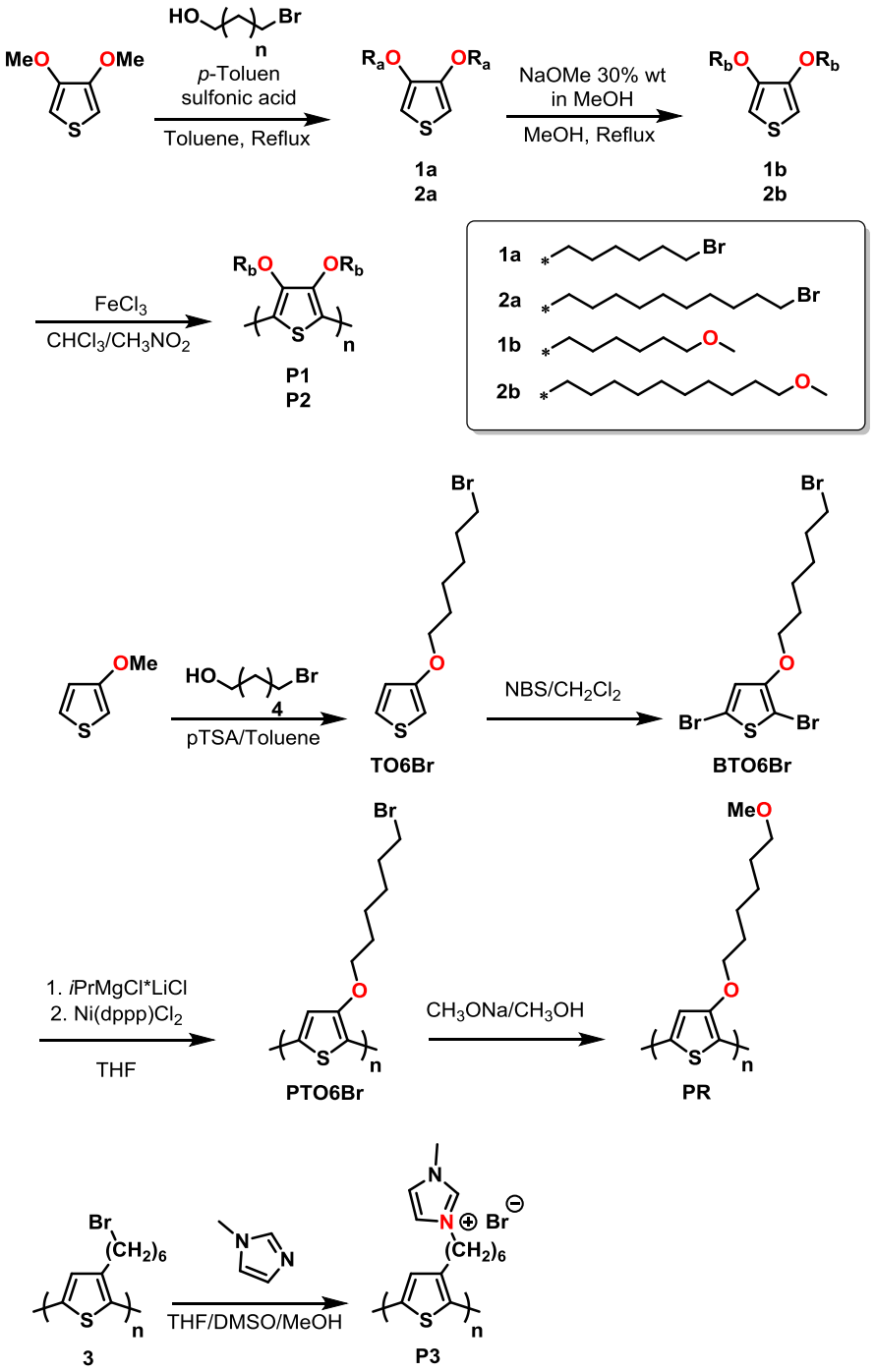

Scheme 1. Synthetic pathway to obtain monomers and polymers.

The cationic water/alcohol soluble polyelectrolyte poly{3-[6-(1-methylimidazolium-3-yl)hexyl]thiophene}bromide (**P3**) was also synthesized by a PPF approach. The regioregular polymeric precursor poly[3-(6-bromohexyl)thiophene] (**3**), obtained as reported in Ref. [13], was reacted with 1-methylimidazolium giving the desired ionic polymer (Scheme 1). As expected, P3 was not soluble in common organic solvents like chloroform or THF, but only in strongly polar solvents (water, methanol, and ethanol) making its weight characterization more complex. However, the structural features of the precursor polymer (like regioregularity and degree of polymerization) are not affected by the substitution reaction and can be derived

from the analysis of its precursor **3**, while the weight data of **P1**, **P2, PR** were obtained through GPC analysis of their soluble fractions (Table 1).

Table 1. Main features of the synthetized polymers.

	Yield (%)	*Dyads (%)*	*Mn (KDa)*[e]	*Xn*[e]	*Đ*[e]
P1	56[a]	100 HH[c]	64.6	189	1.2
P2	64[a]	100 HH[c]	53.7	126	1.3
P3	85[b]	96 HT[d]	44.8	141	1.2
PR	98[b]	96 HT[d]	45.3	187	1.2

[a] Reaction yield; [b] Post-functionalization yield; [c] Head-to-head; [d] Head-to-tail, determined by ^{1}H-NMR spectroscopy; [e] Determined by gel GPC analyses.

2.2 NMR and FT-IR Characterization

Polymers were characterized by ^{1}H-NMR and ^{13}C-NMR analysis in $CDCl_3$ (**P1**, **P2, PR**) and CD_3OD (**P3**). According to the chemical structure, the spectra of **P3** and **PR** show a signal in the aromatic region at 6.96 ppm (P3) and 6.91 ppm (PR), ascribable to the thiophene H-4 aromatic proton (Figure 3SI, signal *m* and Figure 4SI, signal *h*). Moreover, **P3** spectrum shows also the resonances at 9.10, 7.69 and 7.58 ppm (Figure 3SI, signals *d*, *b*, *c*) belonging to N-methyl imidazolium aromatic protons. Moving to higher magnetic fields, **P1, P2** and **PR** show the resonances ascribable to the methylenic protons linked to the thiophenic α-oxygen at 4.11, 4.10 and 4.16 ppm, respectively, methylic and methylenic protons α- to the end-chain oxygen atom in the 3.31-3.39 ppm range, β-CH_2 to the oxygen atom linked to thiophene ring at 1.90 ppm (1.84 ppm for **PR**) and central methylenic protons of the side chains in the 1.7-1.1 ppm range. **P3** spectrum evidences the signal at 4.28 ppm due to -CH_2 α-to the imidazolium group, the signal of the protons of methylic group linked to imidazolium ring at 3.94 ppm, the Th-CH_2 protons at 2.83 ppm and, finally, the remaining resonances of the central methylenic protons of the side chain in the 2.0-1.3 ppm range. The regioregularity of **P3** can be evaluated by the integral ratio of the peak at 2.83 ppm (HT dyads) and the small shoulder at about 2.55 ppm (HH+TT dyads), giving a 96% of HT linkages. Moreover, the presence of a signal at 3.57 ppm (signal *e'*, Fig. 3SI), ascribable to -CH_2Br protons, suggests the incomplete substitution (91% mol) of -Br group by imidazolium. ^{13}C-NMR spectra of the four polymers, reported in Figs. 5SI-8SI, are in good agreement with what reported for ^{1}H-NMR analysis.

Polymers were also characterized by FT-IR spectroscopy using thin films on KBr disk; the recorded spectra are shown in Figure 4 and the characteristic bands are reported in Table S1.

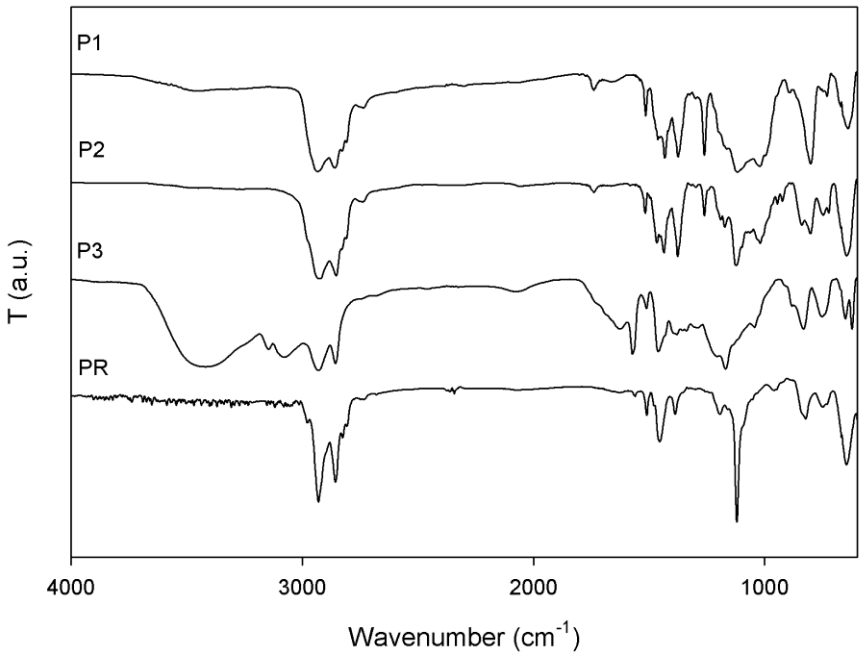

Figure 4. FT-IR spectra of **P1**, **P2**, **P3** and **PR.**

The intensity ratios of the IR bands assigned to the symmetric and antisymmetric stretching modes of the thiophene ring (around 1460 and 1510 cm^{-1}, respectively) are 1.56 for **P1,** 2.51 for **P2**, 1.66 for **PR** and 1.82 for **P3**: the lower values obtained for **P1** and **PR** samples can be related to their more extended conjugation along the polymeric backbone [14], suggesting that the presence of shorter side chains can allow more ordered conformations in the film state. Moreover, polyelectrolyte (**P3**) spectrum evidences the presence of the bands ascribable to the imidazolium functionality (see Table S1) even if a low intensity band at 644 cm^{-1}, ascribable to the stretching of C-Br group of its precursor poly[3-(6-bromohexyl)thiophene] (**3**), is still observable.

3.3 Thermal Analysis

The DSC analysis was performed under nitrogen atmosphere with a heating rate of 10°C/min (Fig. 5).

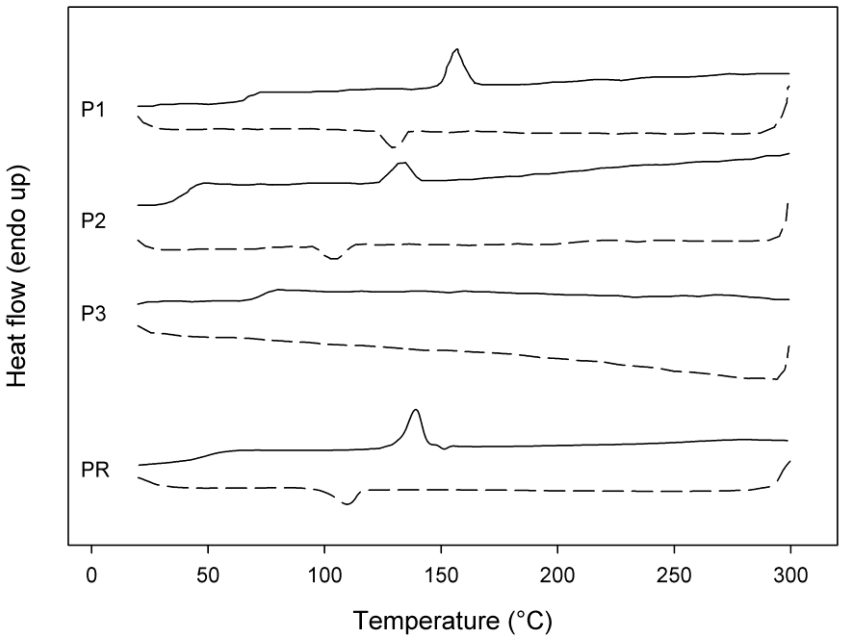

Figure 5. DSC thermograms of **P1**, **P2, P3** and **PR.** Solid line: heating run; dashed line: cooling run.

During the heating scan the thermograms of ED polymers showed one endothermic flexure with a following endothermic peak, and one exothermic peak during the cooling step. While the flexure can be ascribed to the glass-transition temperature (T_g) of the polymer, the peak may be referred to the melting (T_m) process during the heating step, or to the crystallization process (T_c) during the cooling scan (Table 2). **P1** shows transition temperatures and enthalpy (ΔH) values higher than **P2**, thus suggesting a higher cristallinity for the former; the reference polymer **PR** phase-transition temperatures are intermediate between those shown by **P1** and **P2**. Polyelectrolyte (**P3**) sample only shows the T_g, indicating an essentially amorphous structure.

Thermal stability of the polymers was evaluated by TGA analysis under oxidizing atmosphere (air) from room temperature up to 600°C (Figure 6).

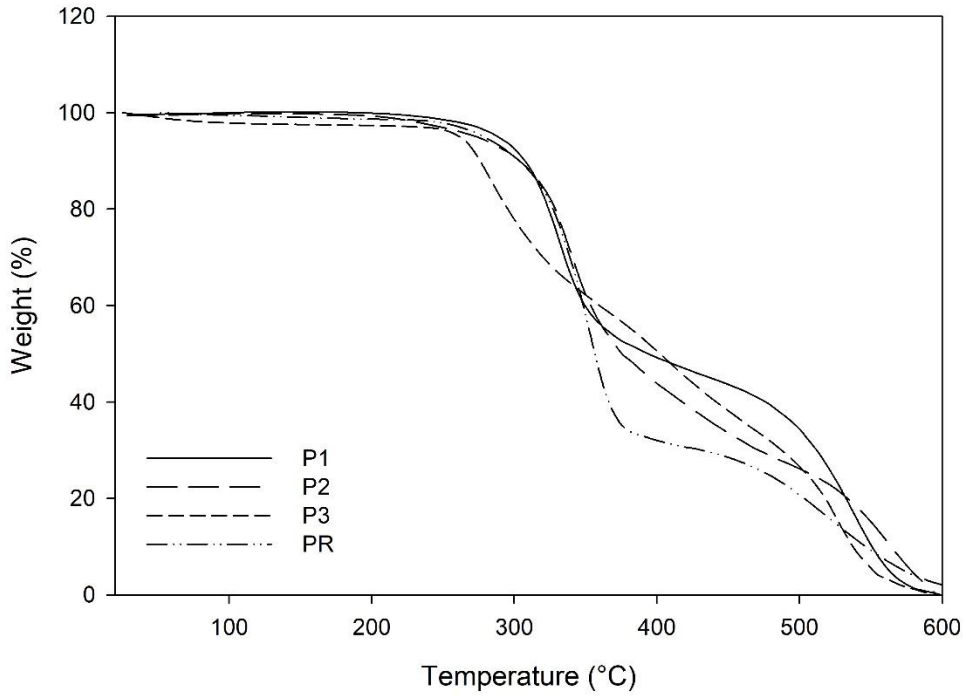

Figure 6. TGA thermograms of **P1**, **P2, P3** and **PR.**

The examined samples show a first weight loss (in the 270-327°C range) ascribable to the scission of the aliphatic chain, followed by the backbone combustion. Polymers stability can be considered suitable for their application in organic solar cells.

Table 2. Thermal characteristics[a] of polymer samples

	T_g (°C)	T_m (°C)	T_c (°C)	ΔH_m (J/g)	ΔH_c (J/g)	T_d (°C)
P1	64	153	126	5.01	4.43	307
P2	40	128	106	3.98	3.23	327
P3	69	-	-	-	-	280
PR	42	135	118	4.87	4.31	270

[a] T_g = glass transition temperature; $T_m/\Delta H_m$ = melting temperature/enthalpy; $T_c/\Delta H_c$ = crystallization temperature/enthalpy; T_d = decomposition temperature.

3.4 UV-Vis and Electrochemical Characterization

P1, P2 and **PR** ED polymers are well soluble in chloroform (see Table 3) and their UV-Vis spectra in this solvent (Figure 7) show an absorption maximum (λ_{max}) at 533 nm for the first two polymers, and at 496 nm for **PR**. On the other hand, the λ_{max} of the cationic polymer **P3** in ethanol undergoes an evident blue-shift to 449 nm.

Table 3. Optical properties of ED polymers (**P1**, **P2, PR**) and polyelectrolyte (**P3**).

	Solvent	***λ_{max} Solution 10^{-5} M (nm)***	***λ_{max} Film (nm)***	***Solubility (mg/mL)***
P1	$CHCl_3$	533	554, 601	10
P2	$CHCl_3$	533	550, 596	13
P3	EtOH	449	511	10
PR	$CHCl_3$	496	538	18

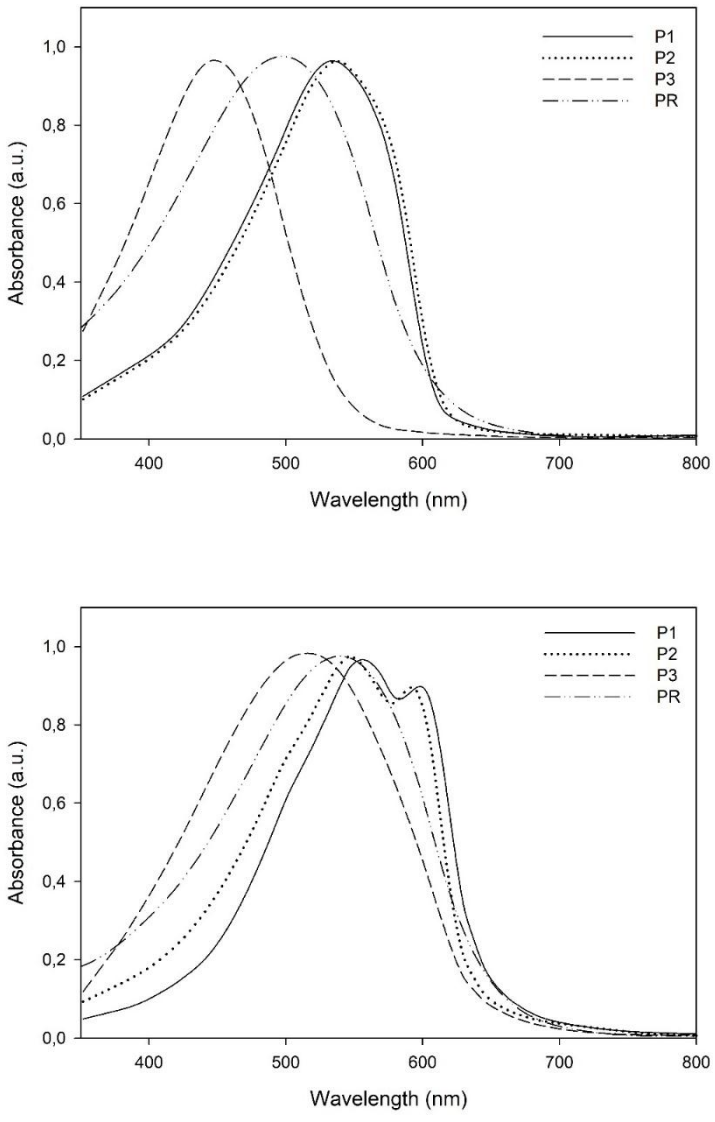

Figure 7. Normalized UV-Vis spectra of the polymers in solution (top) and as thin film (bottom).

When filmed on glass slides, **P1** and **P2** absorption maxima show a bathochromic shift, up to 554 nm for the former and up to 550 nm for the latter (Table 3). Moreover, in the solid state, the structuration of their spectral profiles became evident, with the wavelength of the second absorption maximum at 601 nm (**P1**) and 596 nm (**P2**). It is also noteworthy that the UV-Vis spectrum of a film of the regioregular **PR** sample also undergoes a red-shift of the wavelength of absorption maximum (λ_{max} from 496 in solution to 538 nm in film), even in a lesser extent. Indeed, thanks to the valuable electron-injection properties of the adopted oligoxymethylenic side chains, the electronic density of the polyconjugated backbone is able to increase [15], and this is particularly true for the two polymers with disubstituted thiophenic rings. Finally, polyelectrolyte polymer **P3** in the solid state shows the more blue-shifted λ_{max} (511 nm) when compared to the other synthesized polymers. This fact can be related to the higher steric hindrance of the imidazolium group in the side chain, preventing an efficient stacking of the main chains and reducing the conjugation length of the polythiophenic backbone.

The semi-empirical relation found by Jiang [16] allows us to evaluate the length of conjugated π-electron structure n_L from the wavenumber (ν, cm^{-1}) of the absorption peak (0-1 transition) of the UV-Vis spectrum:

$$\nu = A - B(1/2)^{2/n_L}$$

where A and B are constants determined for the different conjugated polymers. Using the above-mentioned relation, a mean conjugation length of about 17 thiophenic rings for **P1** and **P2** in solution (10 for **PR**) and of about 24 aromatic rings (18 for **PR**) in the solid (film) state can be evaluated. Furthermore, the presence of an evident second maximum suggests the existence of ordered domains in **P1** and **P2** ED polymers, since this absorption is only evident in conformational ordered polythiophenic chains which can form interchain π-π stacking in the solid state [17].

Moreover, the conjugation length of the polymeric backbone, strongly related to the presence of ordered conformers, is inversely proportional to the W parameter, which represents the free exciton bandwidth of the polymeric aggregates. W can be measured by the ratio of the absorbance ascribable to the 0-0 and 0-1 vibronic transitions in the UV-Vis spectra of polythiophenes [18] using the following expression:

$$\frac{A_{0-0}}{A_{0-1}} = \left(\frac{1 - 0.24 W/E_p}{1 + 0.073 W/E_p} \right)^2$$

where E_p is the main intramolecular vibration coupled to the electronic transition (C=C symmetric stretching, 0.18 eV) [19]. From the spectral profiles reported in Figure 7, The calculated W values were 0.023 for **P1** and 0.036 for **P2** sample suggesting, once again, a higher conformational order and crystallinity for the disubstituted polymer bearing shorter (hexyloxy) side chains. Polyelectrolyte and reference polymer spectra, both in solution and in the solid state, do not show any evident vibronic substructure, indicating the absence of long-range ordered domains. For **P3**, this fact can be related to its essentially amorphous microstructure caused by the cumbersome group in side chain while for **PR** to the enhanced

solvating power of the filming solvent ($CHCl_3$) towards both **PR** backbone and side chains, hindering the formation of inter and intrachain associations during the film formation by simple drop-casting, as confirmed by the high solubility of **PR** in the employed chlorinated solvent [[20]].

The electrochemical characterization of polymers was performed using the cyclic voltammetry (CV) technique. Voltammograms were recorded by dropping polymer solutions on a Pt electrode (Figure 8). Considering that the SCE reference electrode has an absolute potential of 4.24 V in acetonitrile solutions [[21]], the energy of the HOMO levels was then estimated according to the equation:

$$E_{HOMO}\ (eV) = -e(E_{ox} + 4.24)$$

Since the reduction potentials of the examined polymers are outside the electrochemical stability window of the electrolyte, LUMO energy levels were calculated indirectly using polymers optical band gaps, evaluated from their UV-Vis spectrum in the film state. Indeed, the onset absorption wavelength (λ_{onset}, nm) can be used to obtain the energy gap (E_g, eV) according to the equation [22]:

$$E_g(eV) = 1240/\lambda_{onset}$$

Being the λ_{onset} of **P1** = 606 nm, **P2** = 630 nm, **PR** = 652 nm and **P3** = 647 nm, the energy gap values reported in Table 3 were directly obtained. Finally, from the equation:

$$E_{LUMO}(eV) = E_{HOMO} + E_g$$

the LUMO level of each synthesized polymer was then obtained.

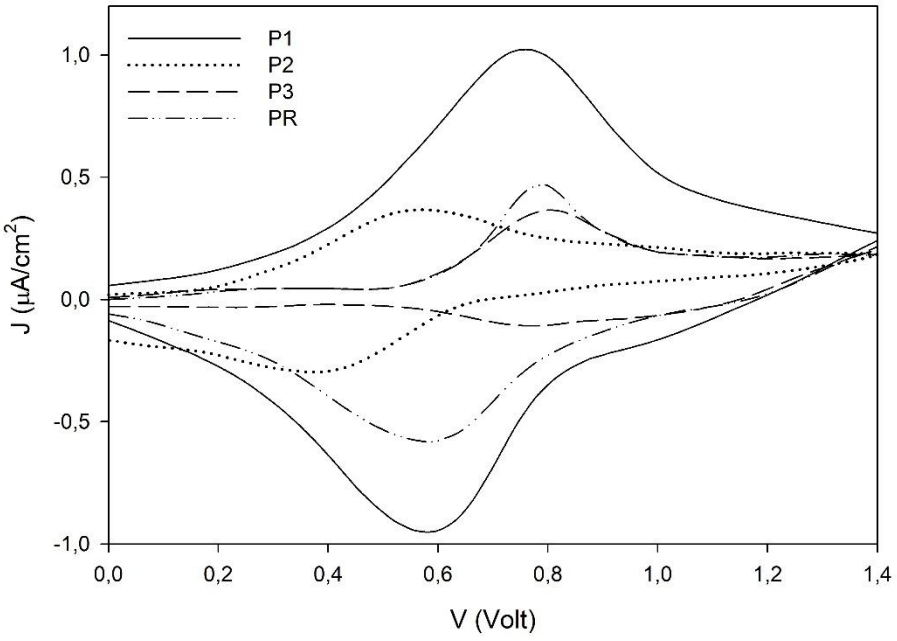

Figure 8. Cyclic voltammetry of different polymers. Electrolyte: hexafluorophosphate ($TBAPF_6$) 0.1M; reference electrode: SCE; scan rate: 100 mV/s.

As reported in Table 4, ED polymers **P1** and **P2** show the lower oxidation potentials, due to the presence of the two electron-donor alkyloxy chains linked to the thiophene ring, followed by **PR**. On the contrary, polyelectrolyte (**P3**) oxidation potential is very similar to that of the commonly used P3HT (-4.8 eV [23]) as the polyelectrolyte bears an alkylic spacer between the thiophene and the ionic group. Indeed, **P3** side chain is devoid of any electron-donor atom directly attached to the thiophene ring, and the methylene groups electronically insulate the 1-methylimidazolium bromide from the polyconjugated backbone.

Table 4. Electrochemical and optical properties of synthesized polymer in thin film.

	E_{ox} (V)[a]	HOMO (eV)	LUMO (eV)	E_g^{optb}
P1	+0.37	-4.61	-2.56	2.05
P2	+0.25	-4.49	-2.52	1.97
P3	+0.61	-4.85	-2.93	1.92
PR	+0.43	-4.67	-2.77	1.90

[a] Onset potential of anodic scan; [b] Optical bandgap in film.

The diagram of energy levels of the materials employed in the examined OSCs, obtained from the data reported in Table 4, is shown in Figure 9.

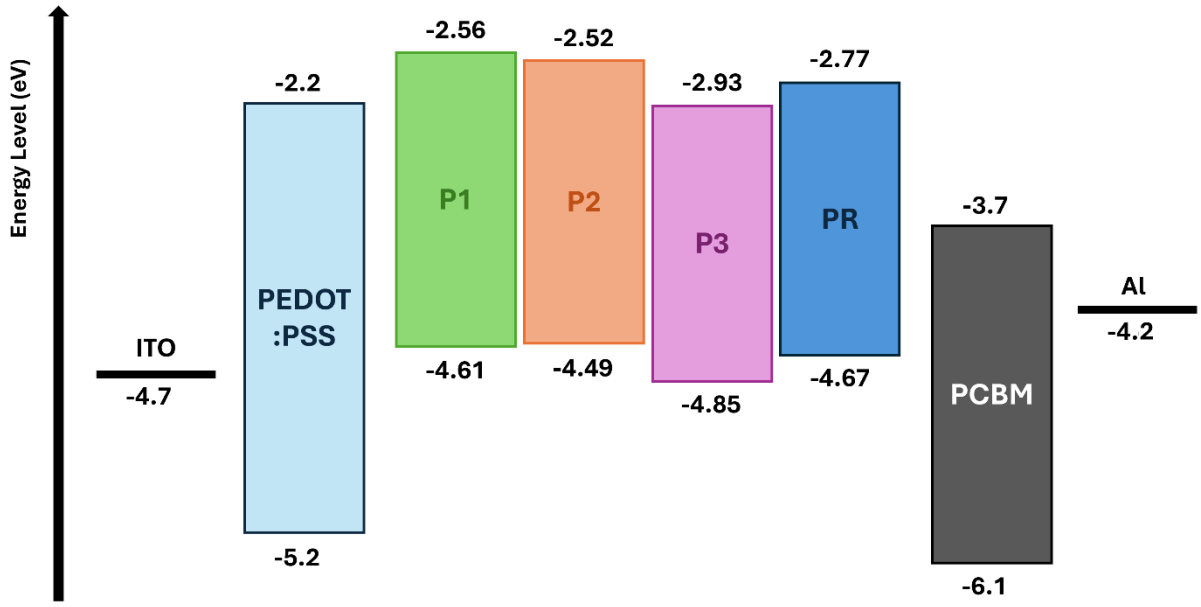

Figure 9. Energy-level diagram of the examined materials [24].

3.5 X-ray diffraction

The study of the molecular arrangement of polymers was performed by X-ray diffraction (XRD) on thick films deposited by Doctor Blade (see Supporting Information) and the recorded patterns are presented in Figure 10. The films of ED polymers **P1** and **P2** showed three characteristic peaks at small angles assigned to (100), (200) and (300) reflections, respectively (Table 5). The first order reflection (100) is ascribable to the distance between polythiophenic chains lying on the same plane while (200) and (300) peaks are induced by multiple X-ray reflections by the film. A similar pattern is shown by **PR** diffractogram. The *d*-spacing corresponds to the distance between the thiophene molecules belonging to the same plane and can be observed in **P1**, **P2,** polyelectrolyte (**P3**) and reference (**PR**) samples at 15.04, 20.55, 18.40 and 14.88 Å, respectively, and it is shorter than the double of the calculated side chain length (22.12, 32.30, 22.98 and 22.10 Å), as determined from density functional theory (DFT) for the B3LYP/6-31G(d) level. This indicates that the side chains are partially interdigitated, providing a three-dimensional chain ordering which can result in enhanced charge-transport properties.[25] Moreover, the less evident peaks at wide angles (2θ = 22.38, 22.15 and 21.63 deg for **P1**, **P2** and **PR**, respectively), partially embedded into the broad amorphous halo and ascribable to the presence of π-π stacking of the thiophene rings in the main chains, once again confirms the semicrystalline nature of the ED polymers suggested by DSC analysis. Polyelectrolyte **P3** does not evidence any peak in this region, according to its essentially amorphous morphology.

The comparison between the mean size of polymer crystallites (L) of the semicrystalline samples, evaluated using Scherrer's equation [26] (Table 5), suggests that **P1** and **PR** polymers are characterized by larger crystalline domains than those observed for **P2**. The crystallization process of the monosubstituted and disubstituted poly(hexyloxy)thiophenes is probably favored by a more planar conformation in the solid state, driven by the shorter length of their side chains if compared with **P2** polymer, bearing two decyloxy side chains. **P3** sample, instead, does not show any evident crystallite since its 3D-order is hindered by the presence of the imidazolium group.

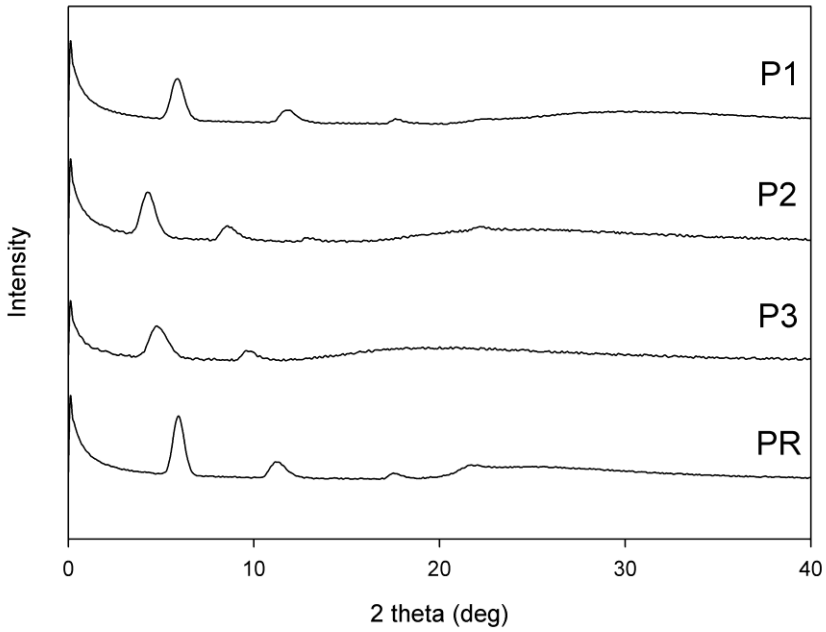

Figure 10. X-Ray diffractograms of polymers in film

Table 5. Structural parameters of polymers

	Low-angle diffractions (2θ)	*High-angle diffractions (2θ)*	*On plane PT chains distances*	*Planes stacking distances*	*Crystallites mean size (L)*
	(deg)	*(deg)*	*(Å)*	*(Å)*	*(nm)*
P1	5.87; 11.78; 17.65	22.38	15.04	3.97	12.15
P2	4.29; 8.59; 12.89	22.15	20.55	4.01	11.08
P3	4.80; 9.64	-	18.40	-	-
PR	5.93; 11.23; 17.56	21.63	14.88	4.11	12.23

3.5 OPV performances

A series of BHJ solar cells with the structure ITO (80 nm)/PEDOT:PSS (100 nm)/ED polymer (**P1**, **P2** or **PR**):PCBM (150 nm)/polyelectrolyte (**P3**) interlayer (10 nm, only samples with asterisk)/Al (50 nm) has been prepared in order to investigate the photoconversion efficiency of the prepared ED polymers as photoactive layers and the effects of the side chain length and of the degree of substitution of thiophene on the final electrical performances [27].

Current density (J) –voltage (V) curves recorded under AM 1.5 one-sun illumination (100 mW/cm^2) are shown in Figure 11 and Figure 12 and the main photovoltaic parameters (short-circuit current density J_{sc}, open-circuit voltage V_{oc}, fill factor FF and power conversion

efficiency PCE), based on the measurements of ten devices of each kind, are collected in Table 6.

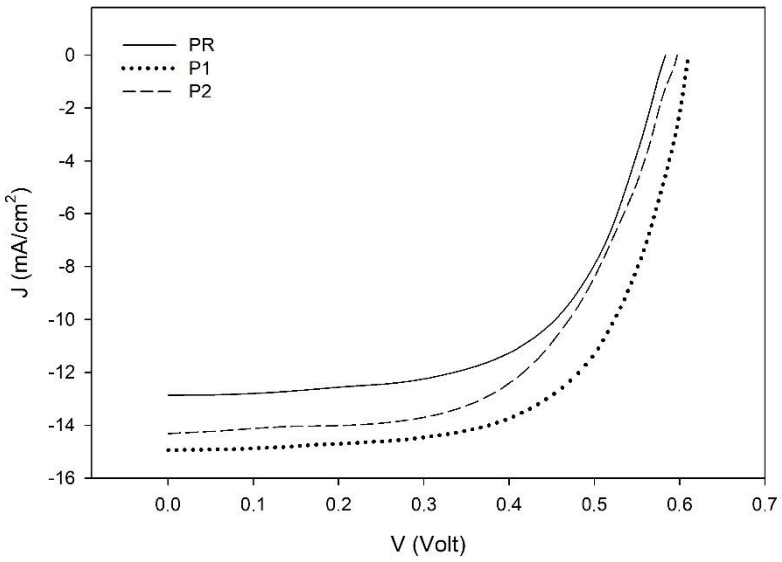

Figure 11. Current density/voltage for the best-performing cells under AM 1.5 one-sun illumination (without cathodic interlayer).

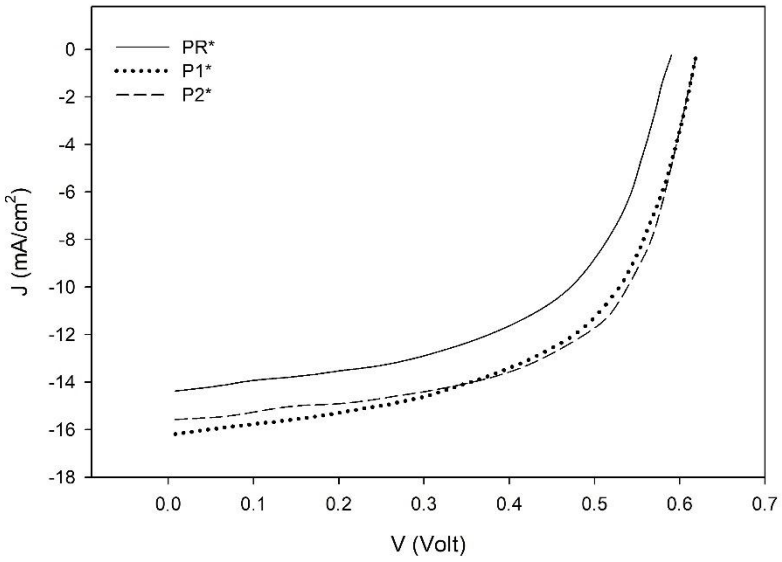

Figure 12. Current density/voltage for the best-performing cells under AM 1.5 one-sun illumination (with **P3** as cathodic interlayer).

Table 6. Photovoltaic characteristics of the obtained cells (average performances taken from ten devices).

Sample	J_{sc} *(mA cm^{-2})*	J_{sc}^{a} *(mA cm^{-2})*	V_{oc} *(V)*	*FF*	*PCE (%)*
PR	12.8±0.5	12.6±0.7	0.58±0.01	0.62±0.02	4.55±0.18
P1	14.9±0.6	14.5±0.9	0.61±0.01	0.62±0.03	5.65±0.22
P2	14.3±0.6	14.0±0.8	0.60±0.01	0.61±0.03	5.24±0.21
PR*	14.3±0.7	14.1±0.9	0.59±0.01	0.61±0.04	5.15±0.20
P1*	16.2±0.9	15.9±1.1	0.62±0.01	0.63±0.05	6.33±0.22
P2*	15.6±0.7	15.4±1.2	0.62±0.01	0.62±0.04	5.98±0.20

* With interlayer [a] From EQE measurements

The photoactive ED polymer/PCBM 1:1 (w/w) blends were subjected to heat treatment (120°C for 45 min under vacuum) to optimize their morphology. We have chosen this heating time since longer periods can result in PCE degradation caused by micron-scale PCBM crystallization which can lead to a progressive segregation of the EA component from the ED polymeric matrix [28]. However, attempts to reduce annealing times resulted in lower power conversion efficiencies.

Best results were obtained using dialkoxyalkylated ED polymers for the photoactive blends, especially **P1** which showed the more red-shifted UV-Vis spectrum when in the film state and a high degree of crystallinity. Indeed, while longer spacers help to increase the solubility of the polymer, they also increase the disorder of the polymer chains, reducing their planarity and crystallinity, as for **P2** sample. Acting on the chemical structure of the monomers therefore proved to be a winning choice, as the reference monosubstituted ED polymer **PR** provided lower photoconversion yields than the two disubstituted samples.

A preliminary attempt was also made to use the polyelectrolyte polymer **P3** as an ED material for the active layer, but the obtained results were not good leading to a PCE around 1.5% for BHJ cells prepared in the same way as the previous ones. Our objective was then to employ polyelectrolyte **P3** as a cathode interlayer (CI), owing to its good solubility in polar solvents that are orthogonal to those employed for ED polymers **P1**, **P2** and **PR** and to its ionic structure. Moreover, ionic polythiophenes applied as cathode interlayers, recently revealed an average increase of efficiency gain by 15-17% in BHJ solar cells, mainly acting on exciton dissociation rate and charge collection efficiency [29]. In the examined cells, the presence of a thin layer of **P3** increased the PCE of the final device by 11%, in agreement with the results reported in literature. The photoluminescence (PL) spectra of the ED polymers and of their blends with PCBM (ED polymer/PCBM 1:1 w/w) in film are shown in Figure S9. The maximum absorption wavelengths of the pristine polymers are at 662, 657 and 661 nm for **P1**, **P2** and **PR**, respectively, and at 661, 660 and 656 nm for **P1***, **P2*** and **PR*** (samples with the cationic interlayer P3). In all the examined samples, the quenching of the fluorescence intensity, ascribable to the intramolecular photoinduced electron-transfer from the polyconjugated backbone to the fullerene moiety [30], is particularly evident.

Furthermore, we recorded external quantum efficiency (EQE) spectra of the cells and the J_{sc} values (Table 5) were obtained by integrating the EQE spectra reported in Figure S10 and Figure S11; we found a good agreement with the J_{sc} values determined by photovoltaic measurements with a mismatch lower than 2%. Moreover, the absorption range of EQE spectra exhibited a red-shift with the use of the cationic layer, which should be beneficial to prepare efficient OPV cells owing to enhanced photon harvesting in the Vis-NIR region.

Photovoltaic results were highly reproducible as shown in Figure S12 and Figure S13 where the statistical errors and the standard box plots of the electrical parameters reported in Table 5, resulting from the measurements of 10 identical devices for each kind, are presented.

To better understand the photovoltaic behavior of the cells, we studied their charge-transport properties by evaluating the hole and electron mobilities using the space-charge-limited current (SCLC) method (Figure S14 and Figure S15) and the obtained values are reported in Table 7.

The SCLC electron mobilities (μ_e) were measured in electron-only devices with a configuration of ITO/PEDOT:PSS/**P1**, **P2** or **PR**/**P3** (when present)/LiF/Al while hole mobilities (μ_h) in a device structure ITO/PEDOT:PSS/**P1**, **P2** or **PR** /**P3** (when present)/MoO_3/Al. The $J^{0.5}$ vs. V curves registered in the dark were then fitted with the Mott-Gurney law [31] and V was corrected for the built-in voltage that arises from the work-function difference between the contacts.

Table 7. Photoelectrical parameters of the examined cells.

Sample	μ_h [a] ($cm^{-2}\ V^{-1}\ s^{-1}$)	μ_e [a] ($cm^{-2}\ V^{-1}\ s^{-1}$)	μ_h/μ_e	R_{SH} (Ohm cm^2)	R_S (Ohm cm^2)	J_{ph}/J_{sat} [b] (%)	n [c]	s [d]
PR	$1.73\ 10^{-4}$	$9.13\ 10^{-5}$	1.9	195±16	4.91±0.23	88.8	0.929	1.21
P1	$1.79\ 10^{-4}$	$9.96\ 10^{-5}$	1.8	266±19	3.25±0.22	92.8	0.941	1.19
P2	$1.76\ 10^{-4}$	$9.81\ 10^{-5}$	1.8	250±18	3.44±0.21	91.3	0.938	1.18
PR*	$1.96\ 10^{-4}$	$1.23\ 10^{-4}$	1.6	301±19	2.55±0.20	93.1	0.933	1.26
P1*	$2.75\ 10^{-4}$	$1.97\ 10^{-4}$	1.4	345±21	1.41±0.18	95.1	0.945	1.25
P2*	$2.70\ 10^{-4}$	$1.80\ 10^{-4}$	1.5	318±20	1.88±0.20	94.2	0.943	1.28

* With **P3** interlayer; [a] Hole mobilities (μ_h) and electron mobilities (μ_e); [b] photocurrent density (J_{ph}) – saturation current (J_{sat}) ratio; [c] exponent of the $J_{sc} = kP^n$ equation, relating the photocurrent to the illumination intensity; [d] scaling factor evaluated by plotting V_{oc} vs. logP (slope = skT/q).

The molecular order of the synthesized polymers endows high hole mobility up to $2.75\ 10^{-4}$ $cm^{-2}\ V^{-1}\ s^{-1}$which is favorable to obtain OSCs with high short-circuit current density (J_{SC}) and fill factor (FF). Moreover, the balance of hole and electron transport can be evaluated from the μ_h/μ_e ratio: this value decreases and closes to 1 when **P3** is used as a cathodic interlayer, suggesting a more optimized charge transport in the photoactive cell [32]. In addition, the

usefulness of the cathodic interlayer for charge transport is also confirmed by the higher shunt (parallel) resistance (R_{SH}) and the lower series resistance (R_S) values measured in the OPV cells when a polyelectrolyte **P3** layer was employed (Table 7).

To investigate the influence of **P3** interlayer on the charge generation efficiency, the photocurrent density (J_{ph}) vs. effective voltage (V_{eff}) curves of the different OSCs were investigated and reported in Figure S16.
J_{ph} was calculated by the difference between the current under illumination (one sun, AM 1.5, 100 mW/cm^2) and that in the dark and V_{eff} was estimated by the difference between the voltage at which $J_{ph} = 0$ (V_0) and the applied voltage (V) [33]. The obtained results are in good agreement with those obtained by J/V curves, since photocurrent density values are almost proportional to the current density values reported before. This is also confirmed by the J_{ph}/J_{sat} ratios (reported in Table 7) where J_{sat} is the saturated photocurrent density measured at short-circuit conditions. Indeed, a higher J_{ph}/J_{sat} ratio indicates that the corresponding OSC can perform a more efficient exciton dissociation and charge generation, resulting in higher J_{sc} and FF measured values [34]. It can also be observed that, at high V_{eff} values ($V_{eff} > 0.5$ V), OSCs prepared with **P1** polymer exhibit a J_{ph} value higher than those of the cells prepared with **P2** or **PR** polymers, suggesting an enhanced exciton generation rate when **P1** is used in the photoactive layer. Furthermore, the comparison between the electrical parameters of the cells prepared with the same ED polymer devoid of **P3** interlayer (**PR**, **P1** and **P2**) and those with the polyelectrolyte layer (**PR***, **P1*** and **P2***) shows the positive effects of the ionic polymer on the charge generation and mobility within the device.

Finally, we have evaluated the importance of charge recombination processes in the examined devices. Recombination phenomena can be evaluated by reporting J_{sc} (short-circuit current density) as a function of the illuminating light intensity P (Figure S17); the relation of P and J_{sc} is $J_{sc} = kP^n$ and, if the exponent n is close to 1, the recombination in the photoactive layers is negligible, owing to an efficient charge transport [32]. In most of the examined cells, n value is close to 1 indicating that the bimolecular recombination in the devices or space-charge effects due to unbalanced charge mobilities is reduced (see Table 7). The small differences between the values of n could be ascribed to the different morphologies of the active layers, as the phase separation degree of the blends plays an important role in determining exciton dissociation, charge transport and collection [35].

Since a polymer functionalized with polar (ionic) functional groups (**P3**) has been employed in the OSCs, the presence of charge-trapping phenomena cannot be excluded. To better evaluate the charge transport properties of the BHJ solar cells, we fitted the relationship of V_{oc} and light intensity as shown in Figure S18.

Indeed, the dependence of V_{oc} from the light intensity (P) gives information about trap state formation, since V_{oc} linearly depends on logP with a slope of skT/q ($1 < s < 2$), where k is Boltzmann's constant, q is elementary charge, s is a scaling factor, and T is Kelvin temperature. Trap-assisted recombination can be identified with a dependence of V_{oc} on light intensity with a slope of 2kT/q (at 300 K), while a slope of kT/q indicates the exclusive presence of bimolecular recombination or surface recombination [36].

From the data reported in Table 7, it is evident that the examined devices, with a slope near to 1 kT/q, have a low trap-assisted recombination. However, s value slightly increases when **P3** interlayer is employed (up to 1.28) and this could be related to the presence of ionic moieties in the structure of the cathodic polymer.

In view of the obtained results, we can conclude that the amount of charge recombination phenomena is however very small for all the examined devices, in addition to show low trap-assisted recombination and balanced charge flow towards the electrodes.

As already stated, the role of the electron transport layer (ETL) is of transporting electrons and blocking the holes; however, its presence can have an impact on the stability of the final device [37] and, with the aim of investigating this point, we have compared the overtime stability of the prepared OPV cells with and without the **P3** layer. Overtime stability of devices was investigated by accelerated ageing after 336 h (two weeks) at 80°C under vacuum. The PCE decrease is reported in Table S2 and in Figure S19. The examined samples show a good thermal stability, with a decrease of the initial PCE ranging from 28% (**P1***) to 35% (**P2**) and the presence of the cathodic interlayer does not seem to have any effect on the device durability.

It is well known that the degree of phase separation between ED and EA components in the active layer has a pivotal role since it directly affects the exciton dissociation and the charge transport and collection to the electrodes. [38] In order to examine the surface nanomorphology of the prepared photoactive blends, atomic force microscopy (AFM) analysis was performed. The following figures report the topographic (top) and the phase images (bottom) of the examined samples (10×10 μm) without (Figure S20) and with (Figure S21) the cathodic interlayer. Figure S22 shows the examined blends.

The films of the pristine blends showed a smooth surface with a root-mean-square (RMS) roughness around 5 nm, suggesting the uniform distribution of the electron-acceptor component ($PC_{61}BM$) in the film. Therefore, at the used ED/EA weight ratio (1:1), polymer chains are stacked together forming homogeneously diffused percolation channels for the transport of charges to the electrodes and the absence of aggregates or large domains of fullerene leads to more effective charge separation thus reducing the electron-hole recombination within the device [39]. Moreover, the addition of a **P3** layer on the outer surface of the OPV cell further enhances smoothness and reduces surface roughness (RMS ranging from 3.9 to 2.2 nm) favoring the final performance of the cell. We can conclude that the appreciable efficiencies obtained with the newly synthesized ED polymers **P1** and **P2**, higher than that shown by the comparison polymer **PR**, arise from balanced charge carrier mobility, reduced recombination phenomena and better morphology of the photoactive layer.

Finally, the knowledge of the synthetic complexity index (SC) for all the employed polymers (see Supporting Information) as well as the PCE values of the examined cells allow us to evaluate their figures of merit (FOM = SC/PCE), which best represent the cost-efficiency balance of a given ED material [10]. FOM values are 4.36 and 4.38 for **P1** and **P2** cells,

respectively, and 5.81 for the reference cell using **PR**. From this simple evaluation, it clearly appears that the cells made with the two disubstituted polyalkyloxythiophenes have the best compromise between polymer synthesis complexity and photoconversion efficiency. This is particularly true not only when their FOM is compared with the reference polymer (**PR**), but also with more recent structures reported in the literature, like poly(thieno[3,4-b]thiophene)s, which show higher PCE values (around 9%) but at the expense of a greater SC (exceeding 60) [40]. However, in this context, the use of the cathodic layer **P3** notably increases the FOM (up to 9.72, 10.01 and 12.30 for **P1***, **P2*** and **PR*** cells, respectively) due to the synthetic complexity of its preparation, hardly justifying its employment and making the large-scale production of the final devices less competitive.

4. Conclusions

In summary, we have developed a new straightforward and effective synthetic strategy to prepare two new symmetrically-disubstituted polyalkyloxythiophenes (**P1** and **P2**) with a simple and economic method when compared with more conventional existing procedures. The properties of the polymers have been carefully examined, especially from the electronic point of view, and compared with those of a more conventional monosubstituted polyhexyloxythiophene (**PR**) used as a reference, showing that the new disubstituted polymers have improved performances and a lower synthetic complexity, highlighting the importance of the molecular architecture of the starting monomers on morphological and photoelectronic properties of the final materials. These materials are therefore excellent candidates to be employed in organic photovoltaic cells, also when a thin layer of the appropriately synthesized conjugated cationic polyelectrolyte (CP) **P3** is inserted between the cathode and the photoactive blend as an electron buffer. However, while the synthetic complexity of cell preparation is raised by using CP, the cationic polymer also enhances the overall photoconversion efficiency of the prepared devices up to a PCE of 6.33%. Indeed, owing to the performing figures of merit, the reported polymers **P1** and **P2** can be further exploited for the large-scale assembly of simple and effective polymeric solar cells.

Acknowledgements

The authors are grateful to the National Recovery and Resilience Plan (NRRP) of Italian Ministry of University and Research, funded by the European Union – NextGenerationEU, project ECOSISTER "Ecosystem for Sustainable Transition in Emilia-Romagna", CUP J33C22001240001, Spoke 2, for the financial support.

References

[1] T. P. Kaloni, P. K. Giesbrecht, G. Schreckenback, M. S. Freund, Polythiophene: from Fundamental Perspectives to Applications, *Chem. Mater.* **2017**, *29,* 10248-10283, https://doi.org/10.1021/acs.chemmater.7b03035.
[2] R. Sorrentino, E. Kozma, S. Luzzati, R. Po, Interlayers for non-fullerene based polymer solar cells, *Energy Environ. Sci.* **2021**, *14*, 180-223, https://doi.org/10.1039/D0EE02503H.
[3] B. X. Dong, C. Nowak, J. W. Onorato, J. Strzalka, F. A. Escobedo, C. K. Luscombe, P. F. Nealey, S. N. Patel, Influence of Side-Chain Chemistry on Structure and Ionic Conduction Characteristics of Polythiophene Derivatives: A Computational and Experimental Study, *Chem. Mater.* **2019**, *31* 1418-1429, https://doi.org/10.1021/acs.chemmater.8b05257.
[4] M. Lanzi, L. Paganin, D. Caretti, New Photoactive Oligo- and Poly-alkylthiophenes, *Polymer* **2008**, *49*, 4942-4948, https://doi.org/10.1016/j.polymer.2008.09.013
[5] P. Schmode, A. Savva, R. Kahl, D. Ohayon, F. Meichsner, O. Dolynchuk, T. Thurn-Albrecht, S. Inal, M. Thelakkat, The Key Role of Side Chain Linkage in Structure Formation and Mixed Conduction of Ethylene Glycol Substituted Polythiophenes, *ACS Appl. Mater. Interfaces* **2020**, *12*, 13029-13039, https://doi.org/10.1021/acsami.9b21604
[6] C. Shi, Y. Y. Yang, Q. Pei, Regioregular Copolymers of 3-Alkoxythiophene and Their Photovoltaic Application, *J. Am. Chem. Soc.* **2006**, *128*, 8980-8986, https://doi.org/10.1021/ja061664x
[7] L. Huo, Y. Zhou, Y. Li, Alkylthio-Substituted Polythiophene: Absorption and Photovoltaic Properties, *Macromol. Rapid. Commun.* **2009**, *30*, 925-932, https://doi.org/10.1002/marc.200800785
[8] S. E. Domínguez, A. Vuolle, M. Cangiotti, A. Fattori, T. Ääritalo, P. Damlin, M. F. Ottaviani, C. Kvarnström, Cationic Imidazolium Polythiophenes: Effects of Imidazolium-Methylation on Solution Concentration-Driven Aggregation and Surface Free Energy of Films Processed from Solvents with Different Polarity, *Langmuir* **2020**, *36*, 2278-2290, https://doi.org/10.1021/acs.langmuir.9b03095
[9] N. N. Linh, T. T. Thuy Duong, N. Hien, V. Q. Trung, Synthesis of polythiophene containing heterocycle on the side chain: a review, *Vietnam J. Chem.* **2020**, *58*, 1-9, https://doi.org/10.1002/vjch.201900184
[10] R. Po, G. Bianchi, C. Carbonera, A. Pellegrino, "All That Glisters Is Not Gold": An Analysis of the Synthetic Complexity of Efficient Polymer Donors for Polymer Solar Cells, *Macromolecules* **2015**, *48*, 453-461, https://doi.org/10.1021/ma501894w
[11] J. He, Z. Su, B. Yan, L. Xiang, Y. Wang, The effects of different side groups on the properties of polythiophene, *Journal of Macromolecular Science, Part A* **2007**, *44*, 989-993, https://doi.org/10.1080/10601320701424321
[12] M. Iovu, E. Sheina, R. Gil, R. D. McCullough, Experimental Evidence for the Quasi-"Living" Nature of the Grignard Metathesis Method for the Synthesis of Regioregular Poly(3-alkylthiophenes), *Macromolecules*, **2005**, *38*, 8649-8656, https://doi.org/10.1021/ma051122k
[13] M. Lanzi, D. Quadretti, M. Marinelli, Y. Ziai, E. Salatelli, F. Pierini, Influence of the Active Layer Structure on the Photovoltaic Performance of Water-Soluble Polythiophene-Based Solar Cells, *Polymers* **2021**, *13*, 1-19, https://doi.org/3390/polym13101640

[14] Y. Furukawa, M. Akimodo, I. Harada, Vibrational key bands and electrical conductivity of polythiophene, *Synth. Met*. **1987**, *18*, 151-156, https://doi.org/10.1016/0379-6779(87)90870-8
[15] H. Hintz, C. Sessler, H. Peisert, H.-J. Egelhaaf, T. Chassé, Wavelength-Dependent Pathways of Poly-3-hexylthiophene Photo-Oxidation, *Chem. Mater*. **2012**, *24*, 2739−2743, https://doi.org/10.1021/cm3008864
[16] R. Qian, Aspects of molecular design of conducting polymers, *Makromol. Chem., Macromol. Symp.* **1990**, *33*, 327-339, https://doi.org/10.1002/masy.19900330128
[17] J. Clark, C. Silva, R. H. Friend, F. C. Spano, Role of Intermolecular Coupling in the Photophysics of Disordered Organic Semiconductors: Aggregate Emission in Regioregular Polythiophene, *Phys. Rev. Lett.*, **2007**, *98*, 206406, https://doi.org/10.1103/PhysRevLett.98.206406
[18] J. Clark, J. F. Chang, F. C. Spano, R. H. Friend, C. Silva, Determining exciton bandwidth and film microstructure in polythiophene films using linear absorption spectroscopy, *Appl. Phys. Lett.* **2009**, *94*, 163306. https://doi.org/10.1063/1.3110904
[19] F. C. Spano, Absorption in regio-regular poly(3-hexyl)thiophene thin films: Fermi resonances, interband coupling and disorder, *Chem. Phys.* **2006**, *325*, 22-35, https://doi.org/10.1016/j.chemphys.2005.08.019
[20] Z. Xu, K. S. Park, J. J. Kwok, O. Lin, B. B. Patel, P. Kafle, D. W. Davies, Q. Chen, Y. Diao, Not all aggregates are made the same: distinct structures of solution aggregates drastically modulate assembly pathways, morphology, and electronic properties of conjugated polymers, *Adv. Mater*. **2022**, *34*, 2203055, https://doi.org/10.1002/adma.202203055
[21] D. Quadretti, M. Marinelli, E. Salatelli, F. Pierini, A. Zanelli, M. Lanzi, Effects of Water/Alcohol Soluble Cationic Polythiophenes as Cathode Interlayers for Eco-Friendly Solar Cells, *Macromol. Chem. Phys.* **2023**, *224*, 2200422, https://doi.org/10.1002/macp.202200422
[22] X. Yan, Y. Liu, Z. Li, S. Shi, W. Shao, X. Kong, Z. Hu, W. Wu, H. Tan, Novel Zinc-porphyrin dyes for dye-sensitized solar cells that enables light capture in the near-ultraviolet and visible range, *Synth. Met.* **2024**, *307*, 117653, https://doi.org/10.1016/j.synthmet.2024.117653
[23] T. V. Richter, C. H. Braun, S. Link, M. Scheuble, E. J. W. Crossland, F. Steizl, U. Wuerfel, Regioregular Polythiophenes with Alkylthiophene Side Chains, *Macromolecules* **2012**, *45*, 5782-5788, https://doi.org/10.1021/ma2026644
[24] Z. Ahmad, M. Awais, M. A. Najeeb, R. A. Shakoor, F. Touati, Poly(3-Hexylthiophene) (P3HT), Poly(Gamma-Benzyl-L-Glutamate) (PBLG) and Poly(Methyl Methacrylate) (PMMA) as Energy Harvesting Materials, in *Smart Polymer Nanocomposites*, D. Ponnamma et al. (eds.), Springer Series on Polymer and Composite Materials, Springer International Publishing AG, **2017**, https://doi.org/10.1007/978-3-319-50424-7_4
[25] R. J. Kline, D. M. DeLongchamp, D. A. Fischer, E. K. Lin, L. J. Richter, M. L. Chabinyc, M. F. Toney, M. Heeney, I. McCulloch, Critical Role of Side-Chain Attachment Density on the Order and Device Performance of Polythiophenes, *Macromolecules* **2007**, *40*, 7960-7965, https://doi.org/10.1021/ma0709001
[26] B. D. Cullity, in *Elements of X-Ray Diffraction*, p. 102 ff, Addison-Wesley Ed., Reading MA, **1978**. ISBN 0-201-01174-3
[27] C. Yang, S. Zhang, J. Hou, Low-cost and efficient organic solar cells based on polythiophene- and poly(thiophene vinylene)-related donors, *Aggregate* **2022**, *3*, e111. https://doi.org/10.1002/agt2.111

[28] N. D. Treat, C. G. Shuttle, M. F. Toney, C. G. Hawker, M. L. Chabinyc, In situ measurement of power conversion efficiency and molecular ordering during thermal annealing in P3HT:PCBM bulk heterojunction solar cells, *J. Mater. Chem*. **2011**, *21*, 15224-15231, https://doi.org/10.1039/C1JM12677F
[29] S. Govaerts, J. Kesters, M. Defour, B. Van Mele, H. Penxten, S. Neupane, F. U. Renner, L. Lutsen, D. Vanderzande, W. Maes, Conjugated ionic (co)polythiophene-based cathode interlayers for bulk heterojunction organic solar cells, *Eur. Polym. J.*, **2017**, *97*, 49-56, https://doi.org/10.1016/j.eurpolymj.2017.09.043
[30] W. L. Ma, C. J. Yang, X. Gong, K. Lee, A. J. Heeger, Thermally Stable, Efficient Polymer Solar Cells with Nanoscale Control of the Interpenetrating Network Morphology, *Adv. Funct. Mater.*, **2005**, *15*, 1617-22, https://doi.org/10.1002/adfm.200500211
[31] F. Yilmaz, in *Conducting Polymers*, Chapter 5, Intech Open Ltd, London, UK, **2016**, https://doi.org/105772/61723, ISBN 978-953-51-2691-1.
[32] Z. Hu, Z. Wang, F. Zhang, Semitransparent polymer solar cells with 9.06% efficiency and 27.1% average visible transmittance obtained by employing a smart strategy, *J. Mater. Chem. A* **2019**, *7*, 7025-7032, https://doi.org/10.1039/C9TA00907H
[33] A. Soultati, M. Verouti, E. Polydorou, K.-K. Armadorou, Z. Georgiopoulou, L. C. Palilis, I. Karatasios, V. Kilikoglou, A. Chronos, A. G. Coutsolelos, P. Argitis, M. Vasilopoulou, Efficient and Stable Air-Processed Ternary Organic Solar Cells Incorporating Gallium-Porphyrin as an Electron Cascade Material, *Nanomaterials*, **2023**, *13*, 2800, https://doi.org/10.3390/nano13202800
[34] H. Feng, X. Song, Z. Zhang, R. Geng, J. Yu, L. Yang, D. Baran, W. Tang, Molecular Orientation Unified Nonfullerene Acceptor Enabling 14% Efficiency As-Cast Organic Solar Cells, *Adv. Funct. Mater.* **2019**, *29*, 1903269, https://doi.org/10.1002/adfm.201903269
[35] Y. Wang, Z. Liang, J. Qin, J. Tong, P. Guo, X. Cao, J. Li, Y. Xia, An Alcohol-Soluble Polymer Electron Transport Layer Based on Perylene Diimide Derivatives for Polymer Solar Cells, *IEEE Journal of Photovoltaics* **2019**, *9*, 1678-1685, https://doi.org/10.1109/JPHOTOV.2019.2941828
[36] S. Wang, Z. Li, X. Xu, G. Zhang, Y. Li, Q. Peng, Enhanced Organic Photovoltaic Performance through Modulating Vertical Composition Distribution and Promoting Crystallinity of the Photoactive Layer by Diphenyl Sulfide Additives, *Adv. Mater. Interfaces*, **2019**, *11*, 7022-7029, https://doi.org/10.1021/acsami.8b20466
[37] S. A. Gevorgyan, I. M. Heckler, E. Bundgaard, M. Corazza, M. Hoesel, R. R. Sondergaard, G. A. dos Reis Benatto, M. Jorgensen, F. C. Krebs, Improving, characterizing and predicting the lifetime of organic photovoltaics, *J. Phys. D: Appl. Phys.* **2017**, *50*, 103001, https://doi.org/10.1088/1361-6463/50/10/103001
[38] J. Sun, X. Ma, Z. Zhang, J. Yu, J. Zhou, X. Yin, L. Yang, R. Geng, R. Zhu, F. Zhang, Dithieno[3,2-b:2′,3′-d]pyrrol Fused Nonfullerene Acceptors Enabling Over 13% Efficiency for Organic Solar Cells, *Adv. Mater.* **2018**, *30*, 1707150, https://doi.org/10.1002/adma.201707150
[39] H. Kim, M. Shin, Y. Kim, Distinct Annealing Temperature in Polymer:Fullerene:Polymer Ternary Blend Solar Cells, *J. Phys. Chem*. **2009**, *113*, 1620-1623, https://doi.org/10.1021/jp809589n
[40] G. Marzano, C. V. Ciasca, F. Babudri, G. Bianchi, A. Pellegrino, R. Po, G. M. Farinola, Organometallic Approaches to Conjugated Polymers for Plastic Solar Cells: From Laboratory Synthesis to Industrial Production, *Eur. J. Org. Chem.* **2014**, *30*, 6583−6614, https://doi.org/10.1002/ejoc.201402226